Synthesis of Iron Oxide Nanostructures by Electrochemical Reduction Method and Their Antifungal Application

A. A. AGALE[1], D.M.SURYAWANSHI[2], S. T. GAIKWAD[1], A. S.RAJBHOJ[1]

[1] Department of Chemistry, Dr.Babasaheb Ambedkar Marathwada University Aurangabad, MS, India.
[2] Department of Chemistry, S.S.G.M. College, Kopargaon, Dist.Kopargaon, M.S., India
Corresponding Author email-ashwiniagale2012@gmail.com.

Abstract

The nanostructured iron oxide (IONPs) were synthesized by electrochemical reduction method using tetra hexyl ammonium bromide as structure directing agent in an organic medium viz. tetra hydro furan and acetonitrile in 1:4 ratio by optimizing current density 14 mA/cm2. Such nanoparticles were prepared using simple electrolysis cell in which the sacrificial anode was as a commercially available iron metal sheet and platinum (inert) sheet acted as a cathode. The synthesized iron oxide nanoparticles were characterized by using ultra violet–visible spectroscopy, X-ray diffraction, scanning electron microscopy, energy dispersive spectroscopy and transmission electron microscope analysis techniques. The nanoparticles were tested for antifungal activity against human pathogens.

Keywords: Electrochemical cell, THAB, Iron oxide nanoparticles, Antifungal activity

Introduction

Metal nanoparticles have received increasingly attention during the last decades because of their original and size dependent properties [1-3].These particles exhibit physical and chemical properties that differ significantly from the bulk or molecular properties of their respective metal [4-6]. It tends to agglomerate strongly due to interlayer attractive van der Waals forces [7]. Therefore, further chemical stabilizer, such as Tetra hexyl am monium bromide (THAB), are frequently required to prevent these kinds of agglomerations [8].

Recently metal NPs exhibit a multiple potential application as well as interest in their fundamental properties including magnetic fluid, magnetic micro device, magnetic resonance imaging, magnetic hyperthermia, drug delivery [9,10].Iron-based nanostructures attract great interest in nanotechnology for their physical and chemical properties [11]. Iron oxides are one of the most important transition metal oxides of technological importance. Remarkable size-dependent optical and structural properties of colloidal iron and iron oxide NPs correspond to the quantum-size effects and electrical structure and the size and crystal structure could be affected by synthesis method [12]. Iron oxide nanoparticles can be synthesized by different methods such as coprecipitation [13], sol–gel [14],combustion processes [15], microemulsion [16], green synthesis [17-19] and electrochemical processes [20].Nanostructured iron oxides are investigated also for applications in catalysis, as active substrates for water splitting, or for the removal of toxic metals from aqueous solutions [21,22]. Since transitional metal oxides are key materials in catalysis, microelectronics, their use in personal and commercial products is in demand which necessitates greater insight towards their ecological impact (as they have an intrinsic toxic property) on their release in the environment. They have many applications against pests, parasites, and pathogens [23-25].

The antifungal effect of metal nanoparticles has been attributed to their small size and high surface to volume ratio, which allows them to attach closely with microbial membranes and is not merely due to the release of metal ions in solution [26].

Experimental

Materials:

All chemicals (up to 99.99% purity) were purchased from Sigma Aldrich. The HPLC grade tetra hexyl ammonium bromide salt THAB and tetrahydrofuran (THF), acetonitrile (ACN) were purchased from Sigma Aldrich and Rankem chemicals and used as such. The sacrificial anode in the form of Iron sheet and platinum sheet as inert cathode having thickness 0.25 mm and purity 99.99% were purchased from Alfa Aesar.

Method:

Iron oxide nanoparticles synthesized by electrochemical method. This method was developed by Reetz in the 1990 [27, 28]. The process makes the use of an inexpensive two electrode set up for 25–30 ml electrolyte solution. Including both oxidation of bulk metal and reduction of metal ions for size selective preparation of tetra alkyl ammonium salt stabilized metal nanoparticles. In the initial experiment we have used a iron metal sheet as anode and a platinum sheet as the cathode. These two electrodes were placed parallel to one another and were separated by 1 cm in 0.01 M solutions of tetra hexyl ammonium salt (THAB) were prepared in ACN/THF (4:1) served as the supporting electrolyte. The electrolysis process was then carried out by applying current of 14 mA/cm^2 for 2 hrs. These nanoparticles after electrolysis were allowed to settle for 1 day. The agglomerated solid sample was separated from the solution by decantation and washed three to four times with THF. The washed samples were then dried under vacuum in desiccators and calcinated at 400°C and used for characterizations.

Characterization techniques:

Structural studies of the synthesized nanoparticles was done. In UV visible spectroscopic analysis supernatant of synthesized nanoparticles were used to record colour and study surface plasmon absorption in the UV-visible region using Jasco UV-Visible Spectroscopy.The powdered X-ray diffraction patterns were obtained out on X-ray powder diffractometer PW-1840, using CuKα radiation (λ = 1.54 A^0). The samples were scanned from 20-820 at the scan rate of 5 x 104 CPS. The scanning electron microscopy study was carried out on JEOL make JSM 63608A microscope to study the morphology of the synthesized nanoparticles.

Transmission Electron Microscopy of synthesized nanoclusters were ultrasonicated in ethanol and then a drop of the dispersed nanoparticles was placed onto a carbon coated 400 mesh copper grid with format coating over it, followed by natural evaporation. Transmission electron microscopic study and electron diffraction were carried out on Philips CM 200kv.

UV–Visible Spectroscopic Analysis

The reduction of iron ions was visibly evident from the color changes associated with it. These IONPs are encapsulated with THAB which is completely removed only after calcinations. The increase in the intensity of the UV band and shifting to higher wavelength may be due to presence of capping agent. As the electrochemical process is a function of current density, the formation of nanoparticles is diffusion controlled and it also depends on the concentration of ions at the electrode surface and in the bulk. The metal nanoparticles exhibit absorption bands or broad regions of absorption in the UV–Vis range due to

the excitation of surface Plasmon resonance (SPR) or interband transitions; these SPR are characteristic properties for the metallic nature of particles. The prominent peak observed at 300 nm in the visible wavelength is due to the absorption of surface Plasmon. A broad peak around 300 nm can be attributed to wide size distribution of particles formed in the solution (Fig. 4).

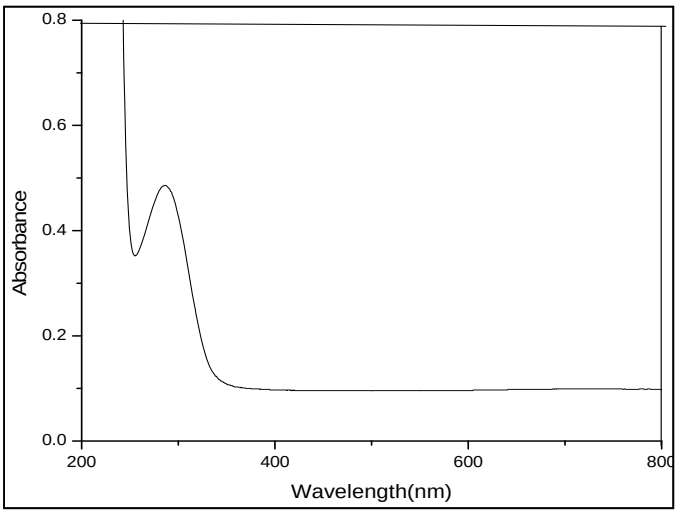

Fig. 4: UV–Vis spectrum for Iron nanoparticles capped with THAB at 14 mA/cm2 current density

XRD:

The phase confirmation of the as-synthesized IONPs was carried out using XRD. X-ray line broadening analysis provides a method of finding bulk average size of coherently diffracting domains. X-ray diffraction (XRD) measurements were performed on all IONPs samples in order to verify the expected crystal structure and estimate average grain sizes. The average crystallite size (D) of solid material can be estimated from X-ray line broadening using the Debye-Scherer equation.

$$D = \frac{K\lambda}{\beta \cos \theta}$$

Where, D =Average particle size, λ= wavelength, θ =diffraction angles, β= FWHM (Full width half maximum).

X-ray diffraction (XRD) pattern of the prepared compound reveals the crystalline nature, phase purity and structure details. Figure 4 show the powder XRD pattern recorded for as prepared iron oxide. The powder X-ray diffraction (XRD) with iron filtered CuKa (l = 1.5405 Å) radiation. Five diffraction peaks (111), (200), (220), (311) and (222) were observed, not only their peak position but their intensity also Matches the standard pattern of FCC type FeO with a wustite phase at space group of Fm3m(225) (Joint Committee on Powder Diffraction Standards (JCPDS) file no.02-1186).

The XRD pattern shows face centered cubic structure (FCC) in Wustite phase No distinct diffraction peak other than those from FCC-Fe was found in the sample. The lattice constant is *a* =b=c were 4.392 Å , matched with JCPDS file no. 02-1186 as shown in fig.2.The broad diffraction peaks are due to nano-size of particles. Maximum intensity peak (111) was used to estimate the crystallite size and it is found to be 36 nm using the Debye–Sherrer method.

This value is consistent with the TEM observations.

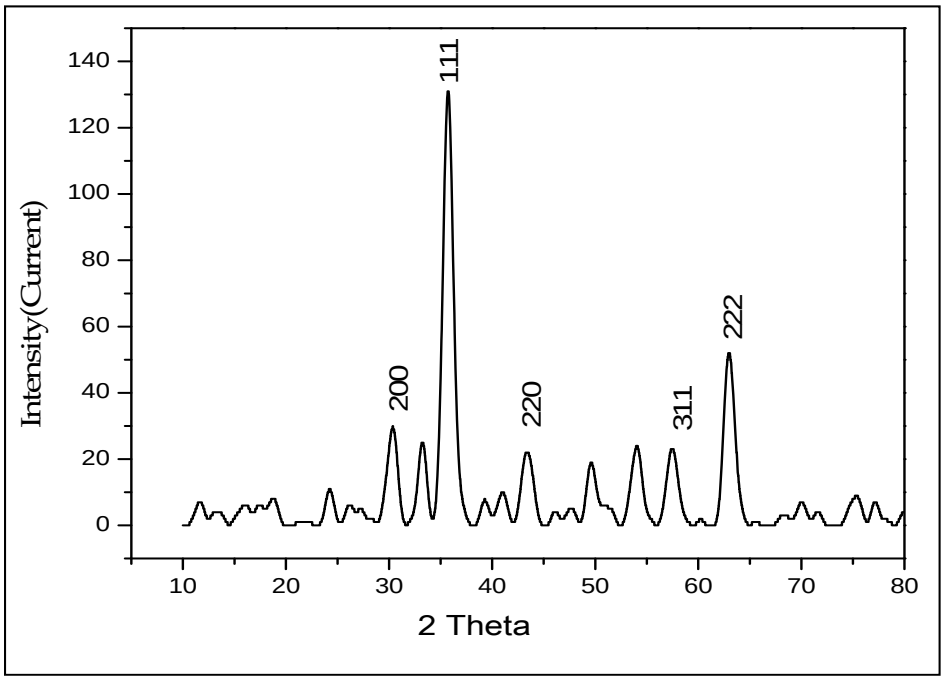

Fig.5: Shows X-ray diffraction pattern of prepared Iron nanoparticles THAB at 14mA/cm.^{2}

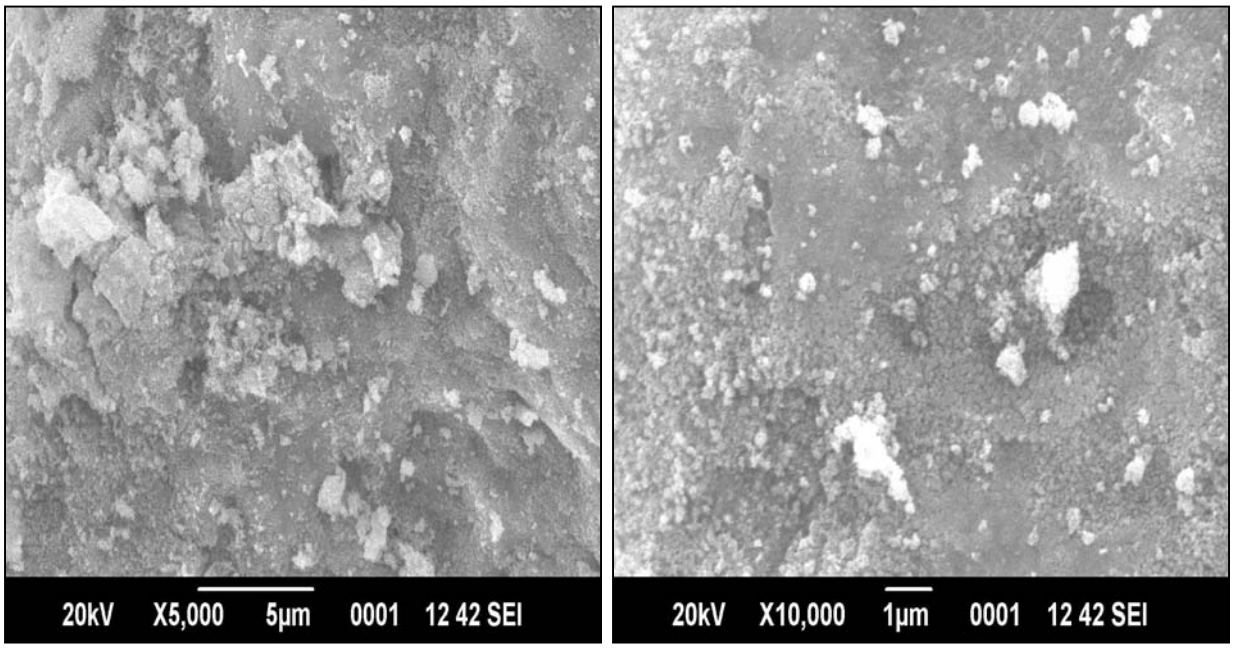

Fig. 6: shows SEM image of iron nanoparticles: 5000 and 10,000 magnification with THAB at 14mA/cm^2.

SEM

SEM experiments are carried out to know the surface morphologies of the samples. Scanning electron (SEM) microscopy imaging technique was utilized to acquire information

about the particle morphology on the nanoscale. Fig .6a shows that these particles have irregular shape and their distribution is not uniform. This is probably due to the partial solubility of the surfactant in the solvent under the given experimental conditions. Fig.6a, b shows the presence of porous nanoparticles that are agglomerated irregularly with close packing. The formation of particle aggregates were observed due to strong interaction among of iron nanoparticles Spheres of a size in the range of 1–10 μm.

EDX

The energy dispersive X-ray analysis (EDX) is performed to know the elemental composition of iron NPs. The elemental composition is presented as the corresponding spectra in **Fig 7** confirmed that the presence of respective nanoparticles as the elementary components. Energy-dispersive spectroscopic study confirmed the presence of Iron oxide. The component oxygen showed in the graph is due to the capping agent attributed to partial oxidation of the nanoparticles during the handling of the sample due to atmospheric oxygen. The composition of atomic % of iron and oxygen which was found to be 91.98 and 8.02 % respectively which clearly shows that formation of pure iron oxide nanoparticles

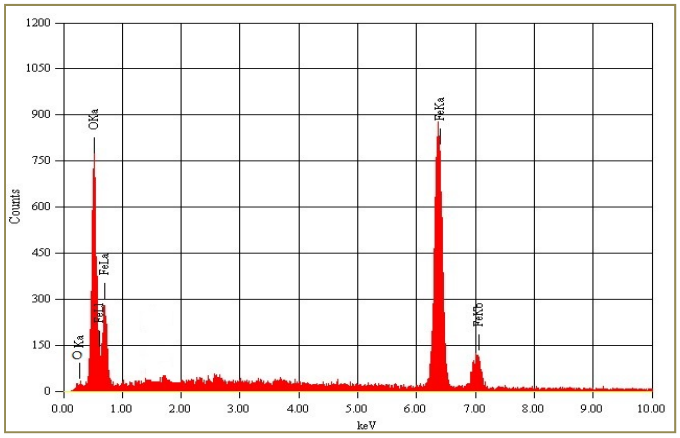

Elements	Atom%	Mass%
Fe	91.98	90.26
O	8.02	9.74
Total	100%	100%

Fig 6: EDX spectrum of FeO nanoparticles and composition of elements.

TEM:

The TEM images depicted in fig. 4a-b are direct morphological observations of Fe NPs micrographs indicate that most particles were fine with various sizes, spherical,cubic and some clusters have also been observed in the Fig.4.a. The average particles size was measured to be 10-50 nm for 14mA/cm^2 current density, which was in good agreement with calculated particles size by XRD analysis. This indicates that grain growth is affected by the reaction time and is favored three dimensionally (i.e. Cubic formation).

Antifungal activity:

The antimicrobial activities of nanoparticles have been attributed to their relatively smaller sizes and high amount of surface-area-to-volume ratio that facilitate interacting closely with membranes of viruses, fungi, and bacteria [27]. In recent years, resistance to commercially available fungicides by phytopathogenic fungi has been increasing and has become a serious problem [28]. Some metal nanoparticles have been studied and proved for their antifungal properties [29-33]. However, few studies are available on the effects of iron nanoparticles on fungal pathogens especially Fusarium causing pathogens.

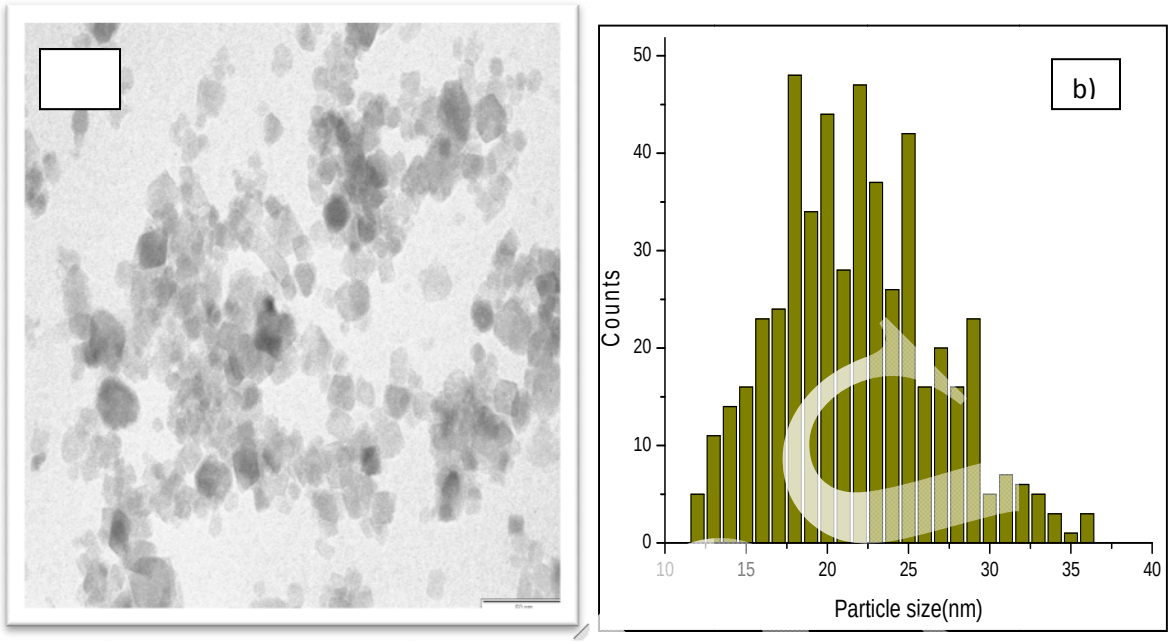

Fig.8 a) TEM images of FeO nanoparticles along with b) particle size histogram of nanoparticles synthesized at current density 14mA/cm^2.

As observed, micro-organism growth log phase has a delayed trend at lower concentrations of Fe NPs loadings. Therefore, it was concluded that complete micro-organism inhibition depends upon the concentrations of NPs and on the number of fungal cells. Indeed, it reflects that Fe NPs have significant biocide effect in reducing micro-organism growth for practical applications.

Table a: In vitro antifungal screening of synthesized Fe NPs against various fungal microorganisms.
In addition,the antimicrobial activity is directly proportional to the nanoparticles concentration. Thus, it can be concluded that iron nanoparticles can be used as fungicide after further confirmatory and biosafety studies.

Materials	Concentration	Diameters of microbial growth inhibition zone (mm)		
		Fungi		
		A.alternata	*A.niger*	*F.oxysporum*
Fe NPs	50 µl	15	14	17
	100 µl	20	18	24
	150 µl	21	20	22
ACN+ THF (4:1)	50 µl	00	00	00
	100 µl	00	00	00
	150 µl	00	00	00
Flucanozole	50 µl	18	16	20
	100 µl	24	23	28
	150 µl	28	30	31

From the results in **Table a,** it can be seen that all samples have better antifungal activity as all sample has zone of inhibition with size more than 9mm. The ACN/THF control did not show any

antifungal activity against the tested fungal strains disc diffusion method, for two different concentrations of Fe nanoparticles i.e.50µl,100µl and 150µl compared with well known antibiotic Flucanozole.

Conclusion

Nanostructured particles of FeO have been successfully synthesized through electrochemical method using THAB as capping agent at 14mA/cm^2 different current densities. XRD results estimate the average particle size as 36 nm for FeO nanoparticles. It also confirms the high degree crystallinity nature of the prepared sample. SEM confirms that the particles are in nano size and the appearances of particles are in irregular polygonal, Cubic and spherical. The XRD analysis of the different iron nanoparticles showed the formation of FeO nanoparticles with Face centered cubic structure. EDX analysis showed the formation of FeO nanoparticles. The TEM confirms that average particle size was 10-50 nm.The prepared iron oxide nanoparticles show excellent antifungal activity and can be used as promising antibacterial agents in wide applications.

Acknowledgements:

The authors are grateful do Department of Chemistry, Dr. Babasaheb Ambedkar Marathwada University, Aurangabad and UGC-SAP-DRS-1 scheme New Delhi for providing laboratory facility. One of the authors (ASR) thankful for financial assistance from Major Research project University Grants Commission, New Delhi. The author (AAA) is also thankful to the University Grants Commission, New Delhi for Rajiv Gandhi National Fellowship.

References:

[1] X. Zhang, R. Zhou, W. Rao, Shanghai 201800 PR China SPRC, and Shanghai 201800 PR C SPR (2006). J. Radioanal. Nucl. Chem. 270, (2), 285–289.
[2] J. Barta, M. Pospısil, and V. Cuba (2010). J. Radioanal. Nucl. Chem. 286, (3), 611–618.
[3] Y. Sun, Q. Wang, S. Yang, G. Sheng, and Z. Guo (2011). J. Radioanal. Nucl. Chem. 290, 643–648.
[4] G. Ozin (1996). Science 271, 920–941.
[5] H. Iida, K. Takayanagi, T. Nakanishi, and T. Osaka (2007). J. Colloid Interface Sci. 314, 274-280.
[6] V. Amendola, P. Riello, and M. Meneghetti (2011). J. Phys. Chem. 115, (12), 5140–5146.
[7] D. Luo, G. Zhang, J. Liu, and X. Sun (2011). J. Phys. Chem. C. 115, 11327–11335.
[8] M. Quintana, E. Vazquez, and M. Prato (2012). Acc. Chem. Res. 46, 138–148.
[9] P. Stoimenov, R. Klinger, G. Marchin, and K. Klabunde (2002). Langmuir 18, 6679.
[10] R. Jong, J. Seung, D. Jong, and C. Sung (2004). Phys. Status Solidi 241, 593.
[11] W. Wu, Q. He, and C. Jiang (2008). Nanoscale Res. Lett. 3, 397–415.
[12] I. Battisha, H. Afify, and M. Ibrahim (2006). J. Magn. Magn. Mater. 306, 211.
[13] J. Toniolo, A. S. Takimi, M. J. Andrade, R. Bonadiman, and C. P. Bergmann (2007). J. Mater. Sci.42, 4785.
[14] V. Chhobro, P. Ayyub, and S. Chattopadhyay (1996). Mater. Lett. 26, 21.
[15] A. Kay, I. Cesar, and M. Graetzel (2006). J. Am. Chem. Soc. 128, 15714–15721.
[16] R. J. Madon and W. F. Taylor (1981). J. Catal. 69, 32–43.

[17] M. Azeez, A. Lateef, T. Asafa, T. Yekeen, A. Akinboro, I. Oladipo, E. Gueguim-Kana, and L. Beukes (2016). J. Cluster Sci., 1–16.
[18] M. Patil, A. Rokade, D. Ngabire, and G. Kim (2016). J. Cluster Sci. 27, (5), 1737–1750.
[19] G. Benelli (2016). a review. Parasitol. Res. 115, (1), 23–34.
[20] A. H. Lu, E. L. Salabas, and F. Schuth (2007). Angew. Chem. Int. Ed. 46, 1222–1245.
[21] H. Zeng and S. Sun (2008). Adv. Funct. Mater. 18, 391–400.
[22] A. Roca, R. Costo, A. Rebolledo, V. Verdaguer, S. Verdaguer, P. Tartaj, T. Gonzalez-Carreno, M.Morales, and C. Serna (2009). J. Phys. D 42, 224002–224012.
[23] Y. Hou, H. Kondoh, M. Shimojo, T. Kogure, and T. Ohta (2005). J. Phys. Chem. B 109, 19094.
[24] K. Murugan, C. Panneerselvam, J. Subramaniam, P. Madhiyazhagan, J. S. Hwang, L. Wang, et al(2016). Environ. Sci. Pollut. Res., 1–15.
[25] K. Murugan, C. Samidoss, C. Panneerselvam, A. Higuchi, and M. Roni (2015). Parasitol. Res. 114,4087–4097.
[26] X. Wang, X. Chen, L. Gao, H. Zheng, M. Ji, C. Tang, T. Shen, and Z. Zhang (2004). J.Mater. Chem.14, 905.
[27] F. Cai, G. Zhang, J. Chen, X. Gou, H. Liu, and S. Dou (2004). Angew. Chem. Int. Ed. 43, 4212.
[28] M. Reetz, W. Helbig, and S. A. Quaiser Active Metals (VCH, Weinheim, 1996), p. 279.
[29] J. R. Moron's, J. L. Elechiguerra, A. Camacho et al. (2005), *Nanotechnology*,16, 10, 2346–2353.
[30] Goffeau, A. "Drug resistance: The fight against fungi", (2008),*Nature*,452:541- 542.
[31] Lemire, J. A., Harrison, J. J. and Turner, R. J. (2013), *Microbiology* 11:371-84.
[32] Singh, M., Kumar, M., Kalaivani, R., Manikandan, S.et.al.(2013), *Bioprocess And Biosystem Engineering* 36:407-15.
[33] Xu, Y., Gao, C., Li, X., He, Y., Zhou, L., Pang, G. and Sun, S. (2013),*Journal of Ocular Pharmacology and Therapeutics* 29:270.